Post-collisional tectonomagmatic evolution in the northern Arabian-Nubian Shi...
Yaron Be'Eri-Shlevin; Yaron Katzir; Martin Whitehouse
Journal of the Geological Society; Jan 2009; 166, Sciences Module
pg. 71

Journal of the Geological Society, London, Vol. **166**, 2009, pp. 71–85. doi: 10.1144/0016-76492007-169.

Post-collisional tectonomagmatic evolution in the northern Arabian–Nubian Shield: time constraints from ion-probe U–Pb dating of zircon

YARON BE'ERI-SHLEVIN[1,2]*, YARON KATZIR[1] & MARTIN WHITEHOUSE[3]
[1]*Department of Geological and Environmental Sciences, Ben-Gurion University of the Negev, Beer Sheva, 84105, Israel*
[2]*Present address: Laboratory for Isotope Geology, Swedish Museum of Natural History, Stockholm, Sweden*
[3]*Laboratory for Isotope Geology, Swedish Museum of Natural History, Stockholm, Sweden*
**Corresponding author (e-mail: Yaron.Beeri@nrm.se)*

Abstract: Ion-probe U–Pb dating of plutonic rocks from the northern Arabian–Nubian Shield in Sinai and southern Israel constrains the timing of late East African batholithic post-collisional calc-alkaline (CA2) magmatism and within-plate alkaline to peralkaline (AL) magmatism to *c.* 635–590 Ma and *c.* 608–580 Ma, respectively. The earliest dated CA2 rocks are slightly deformed to undeformed, indicating that penetrative deformation ceased by *c.* 630 Ma. Within the CA2 suite a change from mafic to felsic magmatism is manifested in most of the region, peaking in a voluminous pulse of granodiorite to granite intrusion at 610–600 Ma. The AL magmatism started contemporaneously with the peak in CA2 felsic activity at *c.* 608 Ma and lasted until 580 Ma. It includes mostly alkaline and peralkaline granites, probably representing variable degrees of differentiation of similar parental magmas. Thus CA2 and AL granites do not represent different tectonic settings, but coeval derivation from variable sources during crustal extension. The majority of rocks dated in this study show minor to non-existent zircon inheritance and thus indicate very minor interaction with previously formed felsic crust. The rare zircon xenocrysts span a typical East African age range (900–607 Ma) and confirm the absence of older crustal components in the juvenile Arabian–Nubian Shield.

Supplementary material: Geochemical and geochronological methods, sample descriptions and data are available at http://www.geolsoc.org.uk/SUP18327.

The Arabian–Nubian Shield (Fig. 1, inset) represents one of the largest exposures of juvenile continental crust on Earth. The shield evolved as the northern segment of the Neoproterozoic East African Orogen (900–530 Ma), and is generally viewed as a collage of juvenile volcanic arc terranes and associated ophiolite remnants that were amalgamated during the assembly of Gondwana (Bentor 1985; Stern 1994, 2002; Stein & Goldstein 1996; Meert 2003; Stoeser & Frost 2006). Geochronological and Nd and Sr isotope studies indicate that much of the Arabian–Nubian Shield formed by net contribution from the mantle with no significant additions from an old silicic crust (Stein & Goldstein 1996; Stern 2002).

At the end of the Neoproterozoic final amalgamation of Gondwana occurred along a vast tract of the East African Orogen and terminated terrane accretion in the Arabian–Nubian Shield. The following tectonomagmatic evolution of the Arabian–Nubian Shield included transition from collision to extension and finally to a stable craton and platform setting (Garfunkel 1999). The basement exposures in Jordan, Israel, the Sinai Peninsula and Eastern Desert of Egypt (Fig. 1, inset) form the northernmost extension of the Arabian–Nubian Shield and shared a common geological history through the main events that followed collision (Stern 1994; Garfunkel 1999; Jarrar *et al.* 2003; Meert 2003; Katzir *et al.* 2007*a*,*b*).

The late evolutionary stages of the northern Arabian–Nubian Shield (650–545 Ma) document the growth and maturation of the continental crust from an orogen to a craton. During this period magmatism changed from calc-alkaline to alkaline and the tectonic setting in which these magmas intruded changed from collision to post-collision, to within-plate extension and finally to a stable platform setting. It is important for our understanding of the nature of this process to resolve these tectonic transitions, but of equal importance is identifying and correlating between the evolution of magmatism and the changing tectonic regime. The nature of transition from calc-alkaline to alkaline magmatism, whether abrupt or gradual, and its correlation to field evidence for initiation of extension in the northern Arabian–Nubian Shield are poorly resolved. Within the rather limited exposures in southwestern Jordan, southern Israel and Sinai geochronological evidence for the timing of this transition is ambiguous. Beyth *et al.* (1994) referred to the transition between calc-alkaline and within-plate alkaline magmatism and suggested that it occurred at *c.* 610 Ma, but their dating was limited to a small area (Timna complex) in southern Israel. Jarrar *et al.* (2003) compiled geochemical and geochronological data for the Jordanian Arabian–Nubian Shield basement rocks and divided them into two suites (Aqaba and Araba suites), based on the *c.* 600 Ma Saramuj unconformity. However, although the Araba suite is characterized by alkaline magmatism, some alkaline granitoids (Yutum suite) were ascribed to the Aqaba suite of mainly calc-alkaline affinity based on their >600 Ma age.

Until recently, geochronology of the late tectonomagmatic stages of the Arabian–Nubian Shield has been based on dating of small detached areas by a variety of methods, mostly Rb–Sr, ^{40}Ar–^{39}Ar and K–Ar, but only rarely U–Pb, making correlation between different rocks and suites difficult. Recent sensitive high-resolution ion microprobe (SHRIMP) U–Pb dating of zircons from the Dokhan Volcanic series of the Eastern Desert of Egypt revealed a significant inherited component, thus question-

Reproduced with permission of the copyright owner. Further reproduction prohibited without permission.

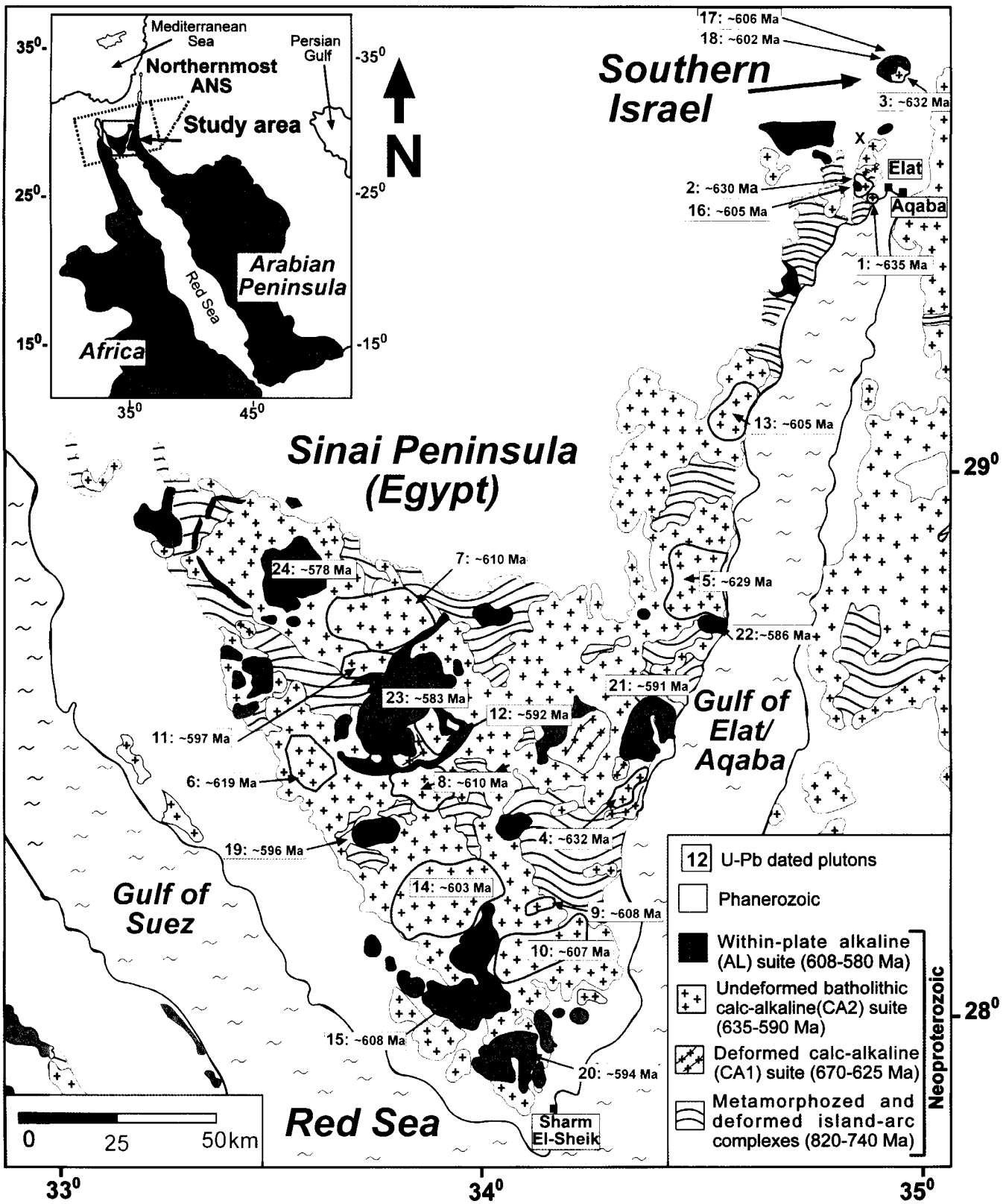

Fig. 1. Simplified geological map of the study area showing the localities of dated rocks (after Eyal *et al.* 1980; Bentor & Eyal 1987). 1, Elat-Shlomo; 2, Elat-Rehavam; 3, Timna Porphyrytic Granite; 4, Shahira; 5, Zreir; 6, Hibran-Miar; 7, Ahdar; 8, Rahba; 9, Sama; 10, Lathi; 11, Sulaf; 12, Abu-K'sheib; 13, Malaha; 14, Girgar; 15, Sahara; 16, Yehoshafat; 17, Timna Alkali Granite; 18, Timna Monzodiorite 19, Umm-Shomer; 20, Sharm; 21, Dahab; 22, Umm-I-Fai; 23, Katharina; 24, Iqna; X, Roded quartz-diorite (not dated in this study). Inset shows the Arabian–Nubian Shield (ANS) Neoproterozoic exposures in eastern Africa and Western Arabia (dark grey) as well as the northernmost segments of the Arabian–Nubian Shield and the study area.

Reproduced with permission of the copyright owner. Further reproduction prohibited without permission.

ing the validity of previous Rb–Sr age determinations of these rocks (Wilde & Youssef 2000). This may also be the case for many other rocks in the northern Arabian–Nubian Shield (see Moussa *et al.* 2008), and thus poses another difficulty. In this study we present new geochronology based on high spatial resolution secondary ionization mass spectrometry (SIMS) dating of zircons from 24 plutons in the Sinai Peninsula (Egypt) and southern Israel, located in a median position in the northern Arabian–Nubian Shield between the Eastern Desert of Egypt to the west and Jordan to the east (Fig. 1). We focus on undeformed plutons that represent the late Neoproterozoic evolution of the northern Arabian–Nubian Shield in this region, from post-collisional to within-plate settings. From the results of this study, compiled with the existing geochronology in the region, we aim to introduce a new time framework for the late Neoproterozoic magmatic activity in this region and refine our understanding of the tectonic processes throughout this time. Our results constrain the end of ductile penetrative deformation in this region, characterize the temporal evolution of calc-alkaline and alkaline magmas, and typify the transition between the two magmatic events. This in turn has important implications for our understanding of the collision to post-collision events and the amalgamation of Gondwana on the wider scale of the East African Orogen.

Geological settings and sample description

The Arabian–Nubian Shield exposures in Sinai and southern Israel are shown in Figure 1. The latest tectonomagmatic events (post *c.* 700-650 Ma) in the northernmost Arabian–Nubian Shield (the northern Eastern Desert of Egypt, Sinai, southern Israel and southwestern Jordan) included voluminous batholithic calc-alkaline (CA) magmatism and less voluminous magmatism of alkaline (AL) character. These magmas intruded the older deformed and metamorphosed island arc complexes of *c.* 820–740 Ma (Bielski 1982; Stern & Manton 1987; Kröner *et al.* 1990; Kolodner *et al.* 2006). Although traditionally CA magmatism is considered as syn- to late orogenic (i.e. older granitoids of the Eastern Desert of Egypt: Stern & Hedge (1985); Moussa *et al.* (2008); the Aqaba suite of Jordan: Jarrar *et al.* (2003)) we infer that two CA suites can be distinguished.

(1) The syncollisional CA1 suite comprises a minor group of older plutons and associated volcanic rocks that have experienced ductile deformation (650–630 Ma: Stern & Manton 1987; Kröner *et al.* 1990; Moussa *et al.* 2008). In the Eastern Desert of Egypt this suite includes trondhjemites, tonalites and granodiorites with minor granites (Moussa *et al.* 2008). In SW Jordan, Sinai and southern Israel, several deformed CA1 gabbro, quartz-diorite and granite intrusions were identified, mainly in association with the older metamorphosed island arc complexes (Stern & Manton 1987; Kröner *et al.* 1990; Jarrar *et al.* 2003; Eyal *et al.* 2004). Importantly, Blasband *et al.* (2000) described metagranites of this phase as part of highly deformed footwall rocks of the Kid core complex in Sinai.

(2) The much more dominant CA2 suite includes slightly deformed to mostly undeformed calc-alkaline intrusions that make up 50–60% of the exposures in the Sinai and southern Israel (Bentor & Eyal 1987). Although most of the CA2 plutons are granodiorites and monzogranites, some minor gabbro and quartz-diorite intrusions also occur. These undeformed plutons postdate accretion and the beginning of the inferred orogenic collapse (core complexes of Blasband *et al.* 2000) and thus are regarded here as batholithic, post-collisional intrusions.

The transition to alkaline (AL) magmatism has been considered by most researchers to be associated with the tectonic transition to an extensional regime manifested by the intrusion of dyke swarms, formation of molasse-filled basins and pronounced erosion (Stern & Hedge 1985; Beyth *et al.* 1994; Moghazi *et al.* 1998; Garfunkel 1999; Jarrar *et al.* 2003; Mushkin *et al.* 2003; Moussa *et al.* 2008). Compositionally, AL magmatism is characterized by intrusion of alkaline to peralkaline high-level plutons (Garfunkel 1999; Katzir *et al.* 2007*a*) and associated bimodal (mafic–felsic) volcanic rocks and dyke swarms of similar age and geochemical affinity (Jarrar *et al.* 2003, 2004; Katzir *et al.* 2006, 2007*b*). Although most dykes are cut by AL plutons, several others intruded at later stages, cutting both AL plutons in Sinai and volcano-conglomerate series and AL plutons in southern Israel. Such observations are also in agreement with those reported in Jordan by Jarrar *et al.* (2003). The alkaline (AL) suite of within-plate or A-type affinity is correlated with the younger granitoids or Granite III of the Eastern Desert of Egypt (Beyth *et al.* 1994; Moghazi *et al.* 1998) and the Araba suite of Jarrar *et al.* (2003).

As the CA2 and AL suites were the main subject of this geochronological study, a brief discussion of the characteristics and geochemical affinities of these two suites in Sinai and southern Israel is presented here. The geochemical composition of CA1 rocks is presented within most diagrams for the purpose of comparison, but in general these rocks follow the same geochemical trends as the CA2 suite (see Figs 2–5). A summary of general characteristics and major and trace element contents for representative samples is available as Supplementary Material.

The CA2 suite includes mainly medium- to coarse-grained, biotite- or biotite- and amphibole-bearing rocks ranging in SiO_2 content from 45 to 75 wt%. Microgranular mafic enclaves of dioritic composition are abundant within many plutons of intermediate to felsic compositions (Bentor & Eyal 1987). The CA2 suite follows a high-K trend in the K_2O v. SiO_2 diagram (Fig. 2a) mainly in intermediate and felsic compositions, and spans metaluminous to peraluminous compositions (A/CNK = 0.7–1.2). On the MALI and #Fe* v. SiO_2 (Fig. 2b and Fig. 2c, respectively) diagrams of Frost *et al.* (2001) the CA2 suite is calc-alkalic to alkali–calcic (in more evolved compositions) and magnesian, respectively. On the HFSE v. FeO*/MgO diagram (Fig. 3a) of Whalen *et al.* (1987) the CA2 plutons plot in the I-type and fractionated I-type fields. In the tectonic discrimination diagrams of Pearce *et al.* (1984) felsic CA2 plutons plot in the volcanic arc granite field (Fig. 3b and c). However in the Rb v. Y + Nb diagram of Pearce (1996) most CA2 plutons cluster within the post-collisional field (Fig. 3b). Mafic and felsic CA2 plutons are moderately enriched in rare earth elements (REE) (ΣREE = 51–190) and show steep REE patterns ($(La/Yb)_n$ = 6–30) with slight to no Eu anomaly on chondrite-normalized diagrams (Fig. 4a). Whereas mafic to intermediate rocks (SiO_2 47–64 wt%) show a more restricted range of REE contents than the felsic rocks (SiO_2 65–76 wt%), both groups show similar chondrite-normalized REE trends (Fig. 4a). Reported U–Pb ages for the CA2 suite in southern Israel are *c.* 634–625 Ma (Beyth *et al.* 1994; Katz *et al.* 1998). Significantly younger ages for the CA2 suite, 625–530 Ma, have been given by the more abundant Rb–Sr age determinations in Sinai and southern Israel (Bielski 1982; Moghazi *et al.* 1998; Eyal *et al.* 2004). Sampled CA2 plutons include medium- to coarse-grained plutons of gabbro to quartz-diorite, granodiorite and monzogranite compositions. Several zoned intrusions, including the Shahira gabbro–diorite layered intrusion (number 4), and the Zreir (number 5) and Hibran-Miar (number 6) plutons of quartz-diorite to granodiorite and monzogranite compositions were also sampled.

Reproduced with permission of the copyright owner. Further reproduction prohibited without permission.

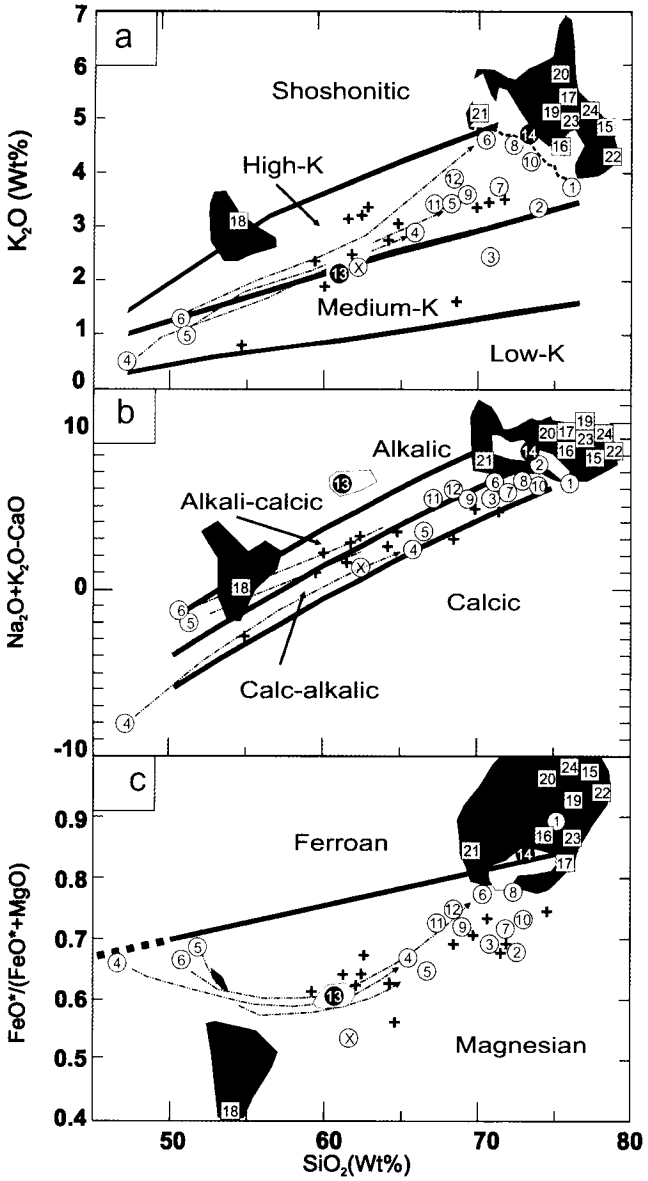

Fig. 2. Major element trends for the CA2 and AL suites of Sinai and southern Israel. (**a**) K_2O v. SiO_2. Field boundaries from Rickwood (1989). (**b**) MALI (modified alkali lime index) v. SiO_2 (after Frost *et al.* 2001). (**c**) FeO*/(FeO* + MgO) v. SiO_2 (after Frost *et al.* 2001). FeO* is total Fe as FeO. Numbers refer to dated plutons (Table 1, Fig. 1), X, Roded quartz-diorite (not dated in this study). White circles, CA2 plutons; grey squares, AL plutons; black circles, transitional plutons. Dashed arrows indicate end-members of zoned plutons. Shaded areas (light grey, CA2; dark grey, AL; white, transitional) and black crosses (+; CA1 suite) are based on a large unpublished dataset kindly shared by M. Eyal and on analyses presented in the Supplementary Material.

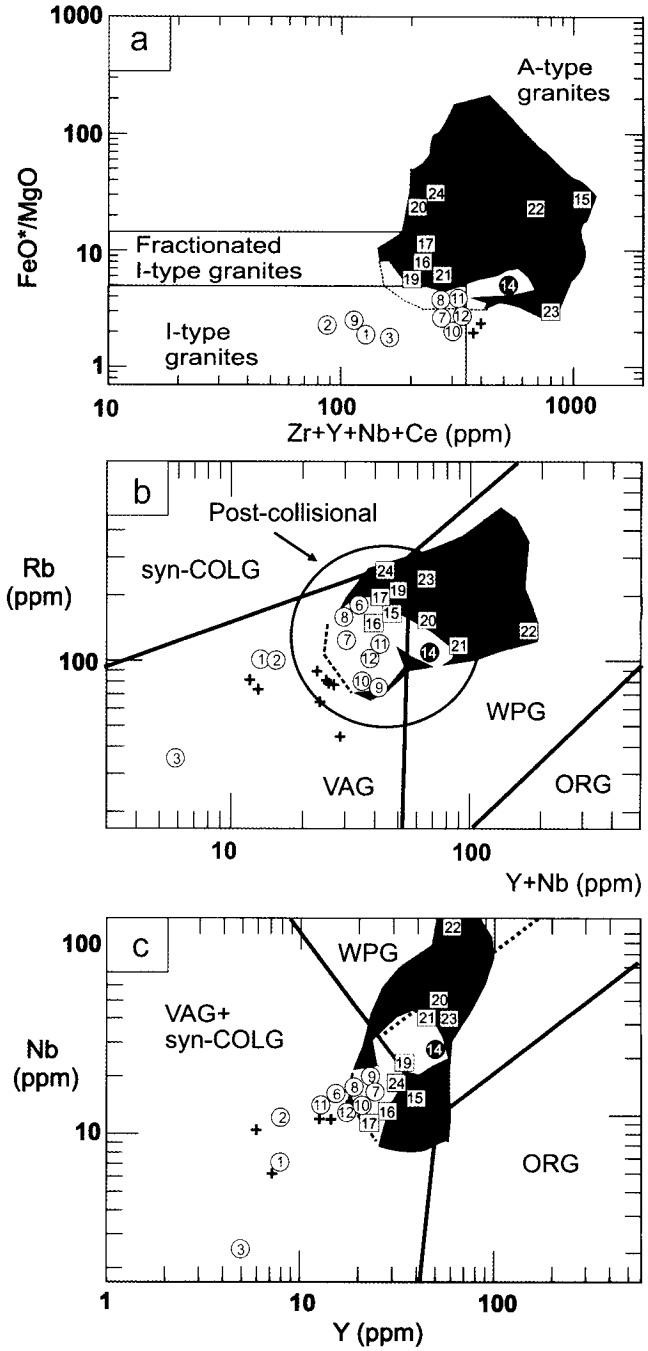

Fig. 3. (**a**) High field strength elements (Zr + Y + Nb + Ce) v. FeO*/MgO for granites of the CA1, CA2 and AL suites (after Whalen 1987). (**b**) Rb v. Y + Nb tectonic discrimination diagram after Pearce *et al.* (1984). Post-collisional field after Pearce (1996). (**c**) Y v. Nb tectonic discrimination diagram after Pearce *et al.* (1984). ORG, ocean ridge granites; syn-COLG, syncollisional granites; VAG, volcanic arc granites; WPG, within-plate granites. Fields and numbering are as in Figure 2.

Plutonic rocks of the AL suite include mainly biotite-bearing syenogranites and alkali feldspar granites, where some of the latter contain Na-amphibole. One small alkaline monzodioritic intrusion was identified in the Timna complex in southern Israel (Beyth *et al.* 1994). Microgranular mafic enclaves are rare to absent. Some of these plutons are associated with bimodal mafic–felsic volcanic rocks, and in some cases are incorporated in ring dyke complexes (Katzir *et al.* 2007*a*). Felsic plutons of this suite have high K contents and the monzodiorite plots in the shoshonitic field in the K_2O v. SiO_2 diagram (Fig. 2a). These are mostly peraluminous to metaluminous (A/CNK = 0.6–1.2) and peralkaline (A/NK = 0.8-1.7) rocks. On the MALI and #Fe* v. SiO_2 diagrams (Fig. 2b and Fig. 2c, respectively) the AL suite is calc-alkalic to alkali–calcic and alkalic, and ferroan, respec-

Reproduced with permission of the copyright owner. Further reproduction prohibited without permission.

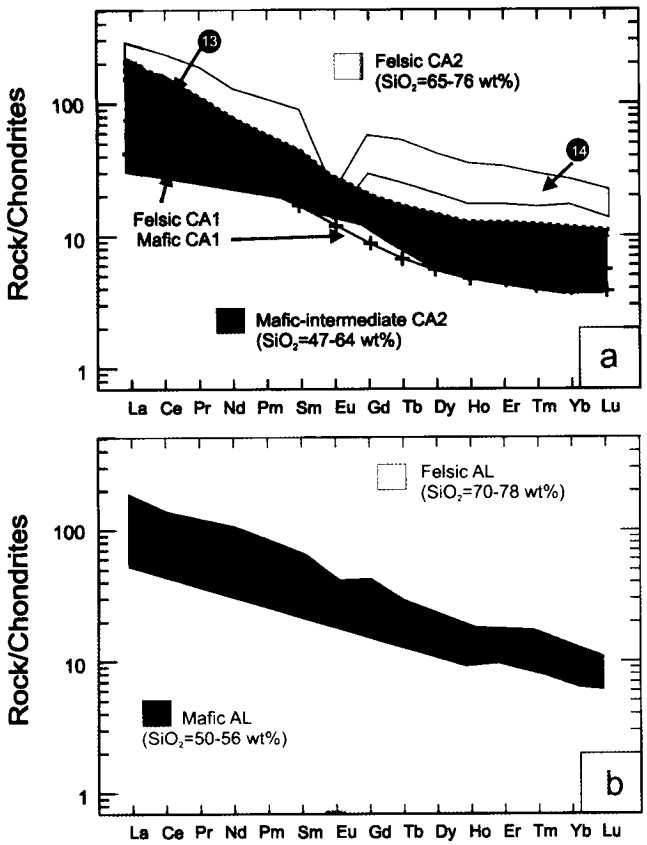

Fig. 4. Chondrite-normalized REE patterns for (**a**) CA2 mafic–intermediate (dark grey) v. felsic (light grey) plutons, (**b**) AL mafic (dark grey) v. felsic (light grey) plutons. Chondrite values are from Sun & McDonough (1989). Location of Malaha (number 13) and Girgar (number 14) plutons is shown in (**a**) as well as representative mafic (gabbro–diorite) and felsic (monzogranite) CA1 intrusions.

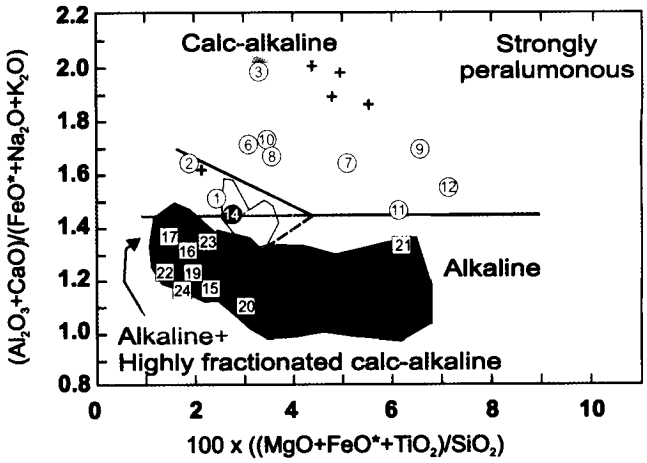

Fig. 5. Major element classification $(Al_2O_3 + CaO)/(FeO^* + Na_2O + K_2O)$ v. $100 \times [(MgO + FeO^* + TiO_2)/SiO_2]$ for felsic CA1, CA2 and AL granitoids (SiO_2 >68 wt%), after Sylvester (1989). Grey horizontal line in the alkaline + highly fractionated calc-alkaline field was extended to decipher between CA and AL plutons.

tively. On the HFSE v. FeO*/MgO diagram (Fig. 3a) the AL suite plots in the A-type and fractionated I-type granite field. On the tectonic discrimination diagrams of Pearce *et al.* (1984) felsic AL plutons plot mostly in the within-plate granite field and slightly extend into the volcanic arc granite field (Fig. 3b and c). AL suite rocks included in this extension, which overlaps some of the CA2 suite rocks, plot within the post-collisional field in Figure 3b. Compared with the CA2 plutons the AL plutons are more enriched in REE ($\Sigma REE = 97–454$) and differ from the CA2 plutons by the monotonous sloping light REE (LREE) and almost flat heavy REE (HREE) ($(La/Yb)_n = 3–24$) patterns and pronounced negative Eu anomalies of felsic compositions (Fig. 4c). Reported U–Pb ages for the AL suite are limited to *c.* 610 Ma determined in the Timna complex of southern Israel (Beyth *et al.* 1994). Rb–Sr ages are more abundant and significantly younger, *c.* 600–530 Ma (Bielski 1982; Mushkin *et al.* 2003). Sampled AL plutons include medium- to coarse-grained, alkaline to peralkaline granites and the Timna monzodiorite of Beyth *et al.* (1994).

Discrimination between highly fractionated calc-alkaline granites of the CA2 suite and alkaline granites of the AL suite is based on the major element discrimination diagram of Sylvester (1989) for rocks with SiO_2 >68 wt% (Fig. 5). In Figure 5 all the highly fractionated CA2 rocks plot above the extension of the horizontal line into the alkaline + highly fractionated calc-alkaline field, and all AL rocks plot below this extension. In two cases assigning the classification criteria to plutons proved problematic. Girgar pluton (number 14) has a median position in most diagrams (Figs 2-5) and is interpreted to represent highly fractionated calc-alkaline magma of the CA2 suite. Malaha pluton (number 13) has some CA2 characteristics (Fig. 2a and c), but plots as alkalic in the MALI diagram (Fig. 2b) and has an anomalous peraluminous composition (A/CNK = 1.7–1.8). It is also characterized by REE concentrations and chondrite-normalized REE patterns that are intermediate between those for the CA2 mafic intermediate and AL mafic plutons (Fig. 4a and b). Thus assigning it to either the CA2 or AL suite is debatable.

Ion-probe U–Pb dating of zircon

U–Pb ages

High-resolution ion probe dating of zircon grains using a CAMECA IMS 1270 was applied to 24 CA2 and AL plutons of Sinai and southern Israel. Concordia diagrams of the dated plutons are shown in Figure 6. For the sake of simplicity, the pluton numbering used in Figures 1–5 is also used in Figure 6. The description of zircon characteristics and a discussion of the assigned ages are summarized in the Supplementary Material. A summary of the U–Pb ages from this study is presented in Table 1. Ages were assigned after omitting from the calculation obvious xenocrystic zircon and young ages interpreted as showing lead loss. In general, we used ^{207}Pb-corrected ($^{238}U/^{206}Pb$) age, representing a projection from assumed common Pb of 0.83 (Stacey & Kramers 1975) through the analysis onto the concordia (as shown schematically by the regression lines in the concordia plots of Fig. 6 (Ludwig 2001)), as this is most appropriate for the age range of these rocks (generally 630–580 Ma). In the case of the Iqna granite (number 24), an alternative $^{207}Pb/^{206}Pb$ age is also presented for a group of high-U zircons (and consequently high radiogenic Pb). These are much less susceptible to problems associated with uncertainty in measurement of common v. radiogenic Pb and are thus considered to produce reliable $^{207}Pb/^{206}Pb$ ages. For some samples, all or most ^{207}Pb-corrected ages were used for determining the mean depending on the mean square weighted deviation (MSWD)

Reproduced with permission of the copyright owner. Further reproduction prohibited without permission.

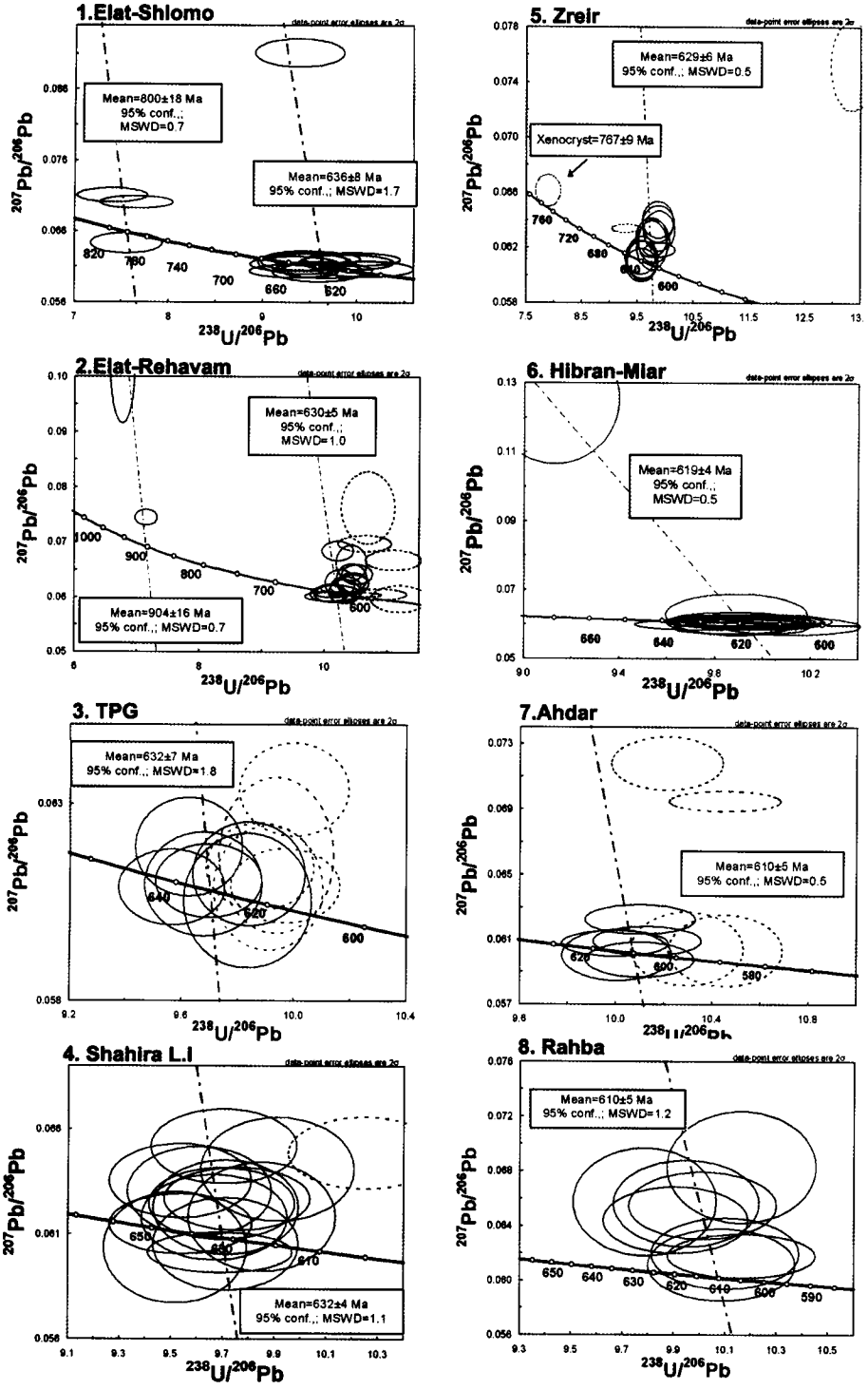

Fig. 6. Terra–Wasserburg concordia diagrams for dated plutons. All age boxes shown are mean ^{207}Pb-corrected ages, except for 24-Iqna, where the mean ^{207}Pb-corrected age is shown for the large concordia, and the inset shows an alternative mean ^{207}Pb/^{206}Pb age. Dashed grey error ellipses in all concordia diagrams represent ages that were not included in the age calculation.

value. We let the MSWD value reach a maximum of 1.8 before omitting younger ages interpreted to represent lead loss.

Summary of U–Pb dating

The U–Pb age spectra from the present study (with the thermal ionization mass spectrometry (TIMS) U–Pb age of the Roded quartz-diorite from Katz *et al.* (1998)) and the areal exposure of each pluton are shown in Figure 7a. The timing of the CA2 and AL magmatism in the northern Arabian–Nubian Shield (Sinai and southern Israel) is constrained to two time spans: *c.* 635–590 Ma and *c.* 608–580 Ma, respectively (Table 1, Fig. 7a).

Within the CA2 suite a general transition from mafic and intermediate to felsic compositions can be distinguished (Fig. 7a). A few felsic intrusions in southern Israel were dated at *c.* 635–630 Ma; however, these are very small in comparison with other CA2 plutons in Sinai (Fig. 7a). Dated mafic (gabbro) magmatism is restricted to small intrusions, whereas larger plutons of intermediate composition are generally zoned complexes including mainly quartz-dioritic to granodioritic variants

Reproduced with permission of the copyright owner. Further reproduction prohibited without permission.

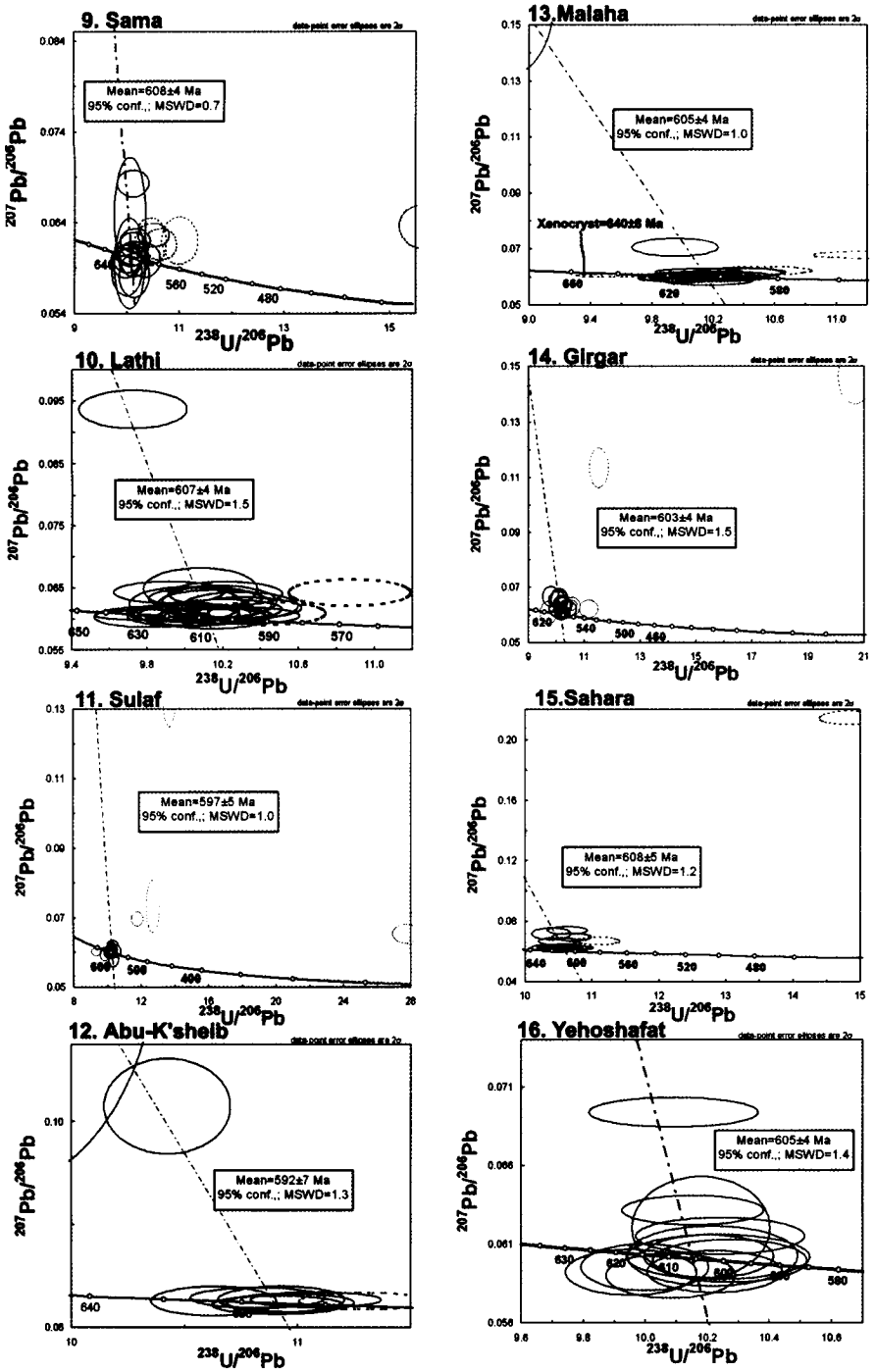

Fig. 6. (*Continued*)

(Fig. 7a). Together with the gabbros, these span an age range of *c.* 635–620 Ma. A major pulse of felsic magmatism of the CA2 suite (granodiorites and monzogranites) occurred at *c.* 610–590 Ma (Fig. 7a). The Girgar granite (number 14), characterized as a highly fractionated calc-alkaline pluton, intruded at the late stages of the CA magmatism. The Malaha pluton (number 13) of quartz-diorite to monzonite composition was dated in this study to *c.* 605 Ma and thus could represent a late mafic–intermediate phase of the CA2 suite or part of the early mafic–intermediate intrusions of the AL suite.

The AL suite includes peralkaline (Na-amphibole-bearing), alkaline (alkali feldspar granites) and syenogranites of ring dyke complexes as well as a small monzodiorite intrusion, all restricted to an age range of *c.* 608–580 Ma. Alkaline and peralkaline granites are indistinguishable by age and cover almost the whole AL age range. The two syenogranites associated with ring dyke complexes (Katharina (number 23) and Iqna (number 24)) were emplaced, however, during the final stages of AL plutonic activity at *c.* 580 Ma (Fig. 7a).

The majority of plutons dated in this study do not have an inherited zircon component, and zircon grains are generally characterized by simple magmatic oscillatory zoning and Th/U

Reproduced with permission of the copyright owner. Further reproduction prohibited without permission.

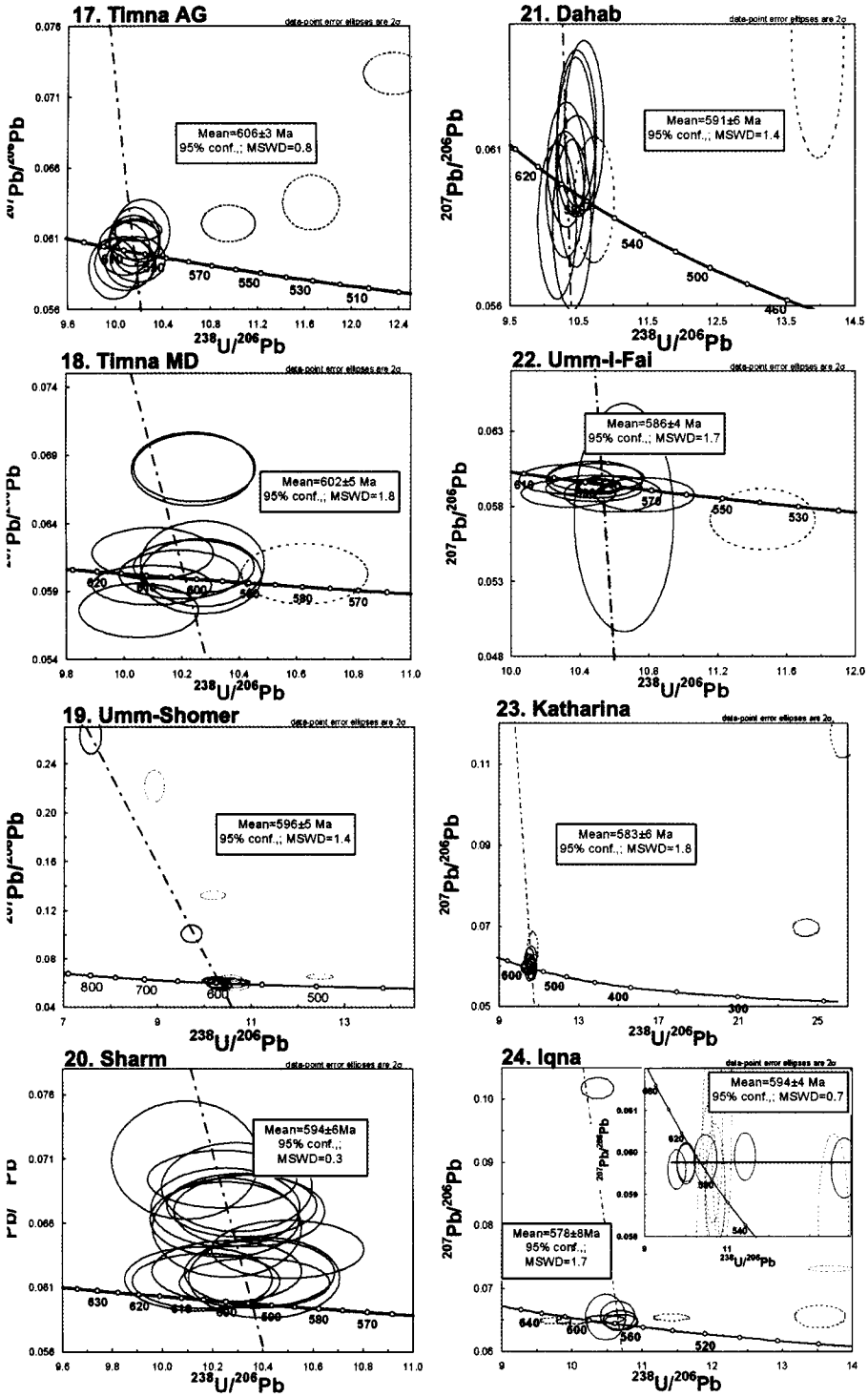

Fig. 6. (*Continued*)

ratios >0.5 typically encountered in magmatic zircon (Hoskin & Schaltegger 2003). Of the 24 dated plutons only three show clear cases of xenocrystic zircons with considerably older age than magmatic age (Elat-Shlomo (number 1), Elat-Rehavam (number 2) and Zreir (number 5) plutons, Table 1), whereas for three other plutons (Sulaf (number 11), Abu-K'sheib (number 12), and Malaha (number 13) plutons, Table 1) inheritance may exist, but is difficult to ascertain because suspected xenocrysts have ages very close to magmatic age. All cases of inheritance (suspected and ascertained) are in plutons of the CA2 suite and xenocrystic zircon range in age from 607 to 900 Ma.

Discussion

Comparison with previous age determinations

Figure 8 shows the zircon U–Pb age distribution of the rocks dated in this study, compiled with zircon U–Pb and Rb–Sr ages in the northernmost Arabian–Nubian Shield reported by others.

Reproduced with permission of the copyright owner. Further reproduction prohibited without permission.

Reproduced with permission of the copyright owner. Further reproduction prohibited without permission.

Table 1. *U–Th–Pb data for CA and AL rocks of Sinai and southern Israel*

Number in Figure 1	Sample	Intrusion	Rock type	n[1]	Zircon structure	U range (av.) (ppm)	Preferred age (Ma)	±95% confidence interval	MSWD	Interpretation
CA2 suite										
1	YE-11	Elat-Shlomo	Monzogranite	15 (3,1)	os-f + sec	340–1630 (670)	636	8	1.7	MCA
					os-f + sec	230–1600 (990)	800	18	0.7	Xenocrysts
2	YE-34	Elat-Rehavam	Monzogranite	22 (2, 12)	os-f + sec	10–3840 (670)	630[2]	5	1.0	MCA
					os-f + sec	190–300 (240)	904	16	1.4	Xenocrysts
3	AG-69	TPG	Monzogranite	11 (0, 5)	os-f + sec	170–550 (350)	632	7	1.8	MCA
4	S-3807	Shahira-LI	Gabbro to qtz-diorite[3]	14 (0, 1)	os-w	770–100 (900)	632	4	1.1	MCA
5	S-4557	Zreir	Qtz-diorite to monzogranite	14 (1, 2[4])	os-f	130–3500 (640)	629	6	1.8	MCA
					os-f	490	767	9		Xenocryst
6	S-2351	Hibran-Miar	Qtz-diorite to granodiorite	15 (0,0)	os-w	20–420 (220)	619	4	0.5	MCA
7	S-2911	Ahdar	Granodiorite to monzogranite	9 (0, 4)	os-f	140–1980 (680)	610	5	0.5	MCA
8	S-2069	Rahba	Granodiorite—Qtz-monzonite	8 (0, 0)	os-f + sec	60–260 (120)	610	5	1.2	MCA
9	S-3704	Sama	Quartz-monzonite–monzogranite	18 (0, 6)	os-f + sec	80–740 (240)	608	4	0.7	MCA
10	S-1610	Lathi	Monzogranite[5]	21 (0, 2)	os-f	70–1100 (270)	607	4	1.5	MCA
11	S-2199	Sulaf	Granodiorite–monzogranite–monzonite	14 (1, 5[6])	os-f + sec	90–1190 (360)	597	5	1.0	MCA
						350	650	9		Xenocryst?
12	S-2695	Abu-K'sheib	Qtz-monzonite–monzogranite	9 (1, 1)	os-f + sec	14–390 (250)	592	7	0.5	MCA
					os-f	100	607	7		Xenocryst
Transitional plutons										
13	S-4917	Malaha	Qtz-diorite–monzonite	18 (1, 2)	os-f + sec	190–380 (350)	605	4	1.0	MCA
					os-f + sec	1690	640	8		Xenocryst?
14	S-1561	Girgar	Monzogranite	18 (0, 5[7])	os-f + sec	50–600 (190)	604	4	1.1	MCA
AL suite										
15	S-1542	Sahara	A- fel granite[8]	13 (0, 2)	os-f + sec	210–1200 (540)	608	5	1.2	MCA
16	AG-81	Yehoshafat	A-fel granite	12 (0, 0)	os-f	50–480 (200)	605	4	1.4	MCA
17	AG-68	TAG	A-fel granite	13 (0, 3)	os-f	90–850 (230)	606	3	0.8	MCA
18	AG-77	TMD	Monzodiorite	10 (0, 1)	os-w + sec	70–300 (170)	602	5	1.8	MCA
19	S-1885	Umm-Shomer	Syenogranite	15 (0, 8)	os-f	70–400 (180)	596	5	1.4	MCA
20	S-1518	Sharm	A-fel granite	15 (0, 0)	os-f + sec	90–160 (120)	594	4	0.7	MCA
21	S-3896	Dahab	Syenogranite	10 (0, 2)	os-f + sec	80–250 (140)	591	6	1.4	MCA
22	S-4403	Umm-I-Fai	A-fel granite[8]	9 (0, 1)	os-f + sec	300–2000 (1160)	586	4	1.7	MCA
23	DV-82-87	Katharina	Syenogranite	11 (0, 2)	os-f	40–1450 (330)	583	6	1.8	MCA
24	YS-503	Iqna	Syenogranite	13 (0, 7)	os-f + dark	70–7010 (24230)	578	8	1.7	MCA
				6	dark	2540–7010 (4840)	594[9]	6	0.3	MCA[9]

A-fel, alkali feldspar; MCA, magma crystallization age; os-f, fine oscillatory zoning; os-w, widely spaced oscillatory zoning; Qtz, quartz; Sec, sector zoning; Shahira-LI, Shahira layered intrusion; TAG, Timna alkali granite; TMD, Timna monzodiorite; TPG, Timna porphyritic granite.

[1]Unless stated differently, $x(y, z)$ refers to x, the total number of analyses; y, the number of xenocrysts; and z, the number of analyses interpreted to show lead loss, where y and z were not used for age calculation.

[2]Our calculation used only eight analyses although the oldest 13 (excluding the two xenocrysts) ^{207}Pb-corrected ages yielded a weighted mean age of 623.9 ± 5.3 Ma, MSWD = 1.8.

[3]S-3807 is a felsic layer of granodioritic composition.

[4]One analysis was omitted because of high U content.

[5]S-1610 is a monzonite rim variant of the pluton.

[6]One older rim analysis of *c.* 660 Ma was omitted because it was significantly older than two core analyses of that grain.

[7]One older rim analysis of *c.* 630 Ma was omitted because it was significantly older than a core analysis of that grain.

[8]Na-amphibole-bearing granites.

[9]$^{207}Pb/^{206}Pb$ alternative age calculated for high-U grains only.

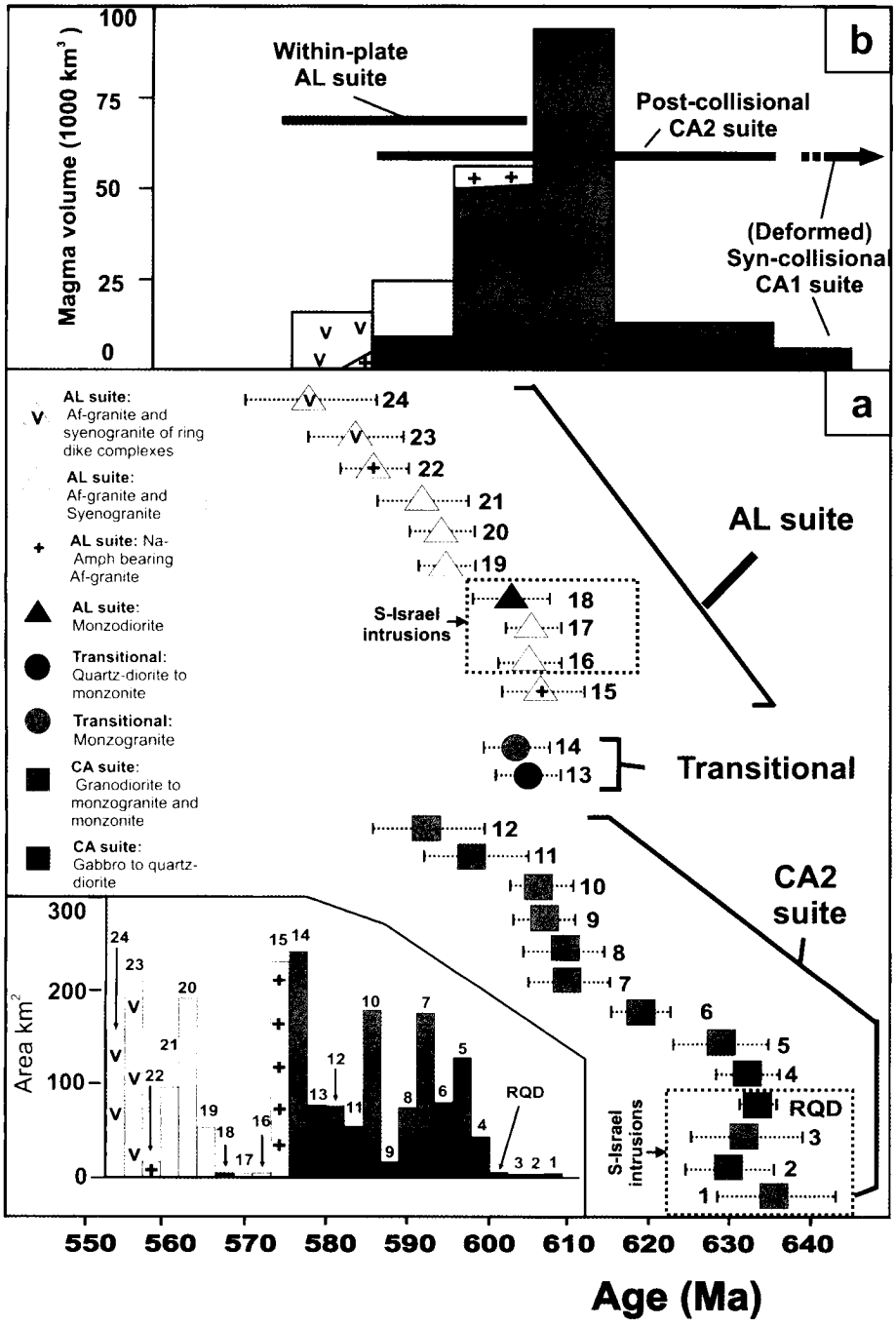

Fig. 7. (**a**) Ion probe U–Pb age distribution of rocks dated in this study and TIMS U–Pb age for the Roded quartz-diorite (RQD, after Stein & Goldstein 1996; Katz *et al.* 1998), and the surface exposure of each pluton. Numbers as in Figure 1 and Table 1. (**b**) Estimated magma volume v. age in Sinai and southern Israel during the time interval 650–570 Ma. Af, alkali feldspar; Amph, amphibole.

These include rocks from the northern part of the Eastern Desert of Egypt, the Sinai Peninsula, southern Israel and southwestern Jordan.

Dated rocks from the Timna complex (i.e. Timna porphyrytic granite (number 3), Timna monzodiorite (number 18) and Timna alkali granite (number 17); Table 1, Fig. 7a) correlate well with single-zircon evaporation ages reported by Beyth *et al.* (1994) for the same rocks. The 634 ± 2 Ma and *c.* 630 Ma U–Pb TIMS ages of the Roded quartz-diorite from southern Israel (Fig. 1) reported by Katz *et al.* (1998) and Stein & Goldstein (1996), respectively, are comparable with the earliest ages of CA2 rocks in this study (Figs 7a and 8). Reported U–Pb ages in southwestern Jordan and the northern Eastern Desert of Egypt are generally in agreement with the range of U–Pb ages in this study (Fig. 8), although they show a somewhat more restricted age range for rocks correlative to the CA2 and AL suites, probably because of the small number of U–Pb ages determined in these areas (Moussa *et al.* 2008).

Reported Rb–Sr ages of post-collisional calc-alkaline and within-plate alkaline rocks in the northernmost Arabian–Nubian Shield span an age range of *c.* 620–530 Ma (Bielski 1982; Stern & Hedge 1985; Moghazi *et al.* 1998; Jarrar *et al.* 2003, and references therein). Comparing the U–Pb ages from this study with several reported Rb–Sr ages for the same plutons (Lathi (number 10), Dahab (number 21), Elat-granites (numbers 1 and 2), and Katharina (number 23) of this study compared with the

Reproduced with permission of the copyright owner. Further reproduction prohibited without permission.

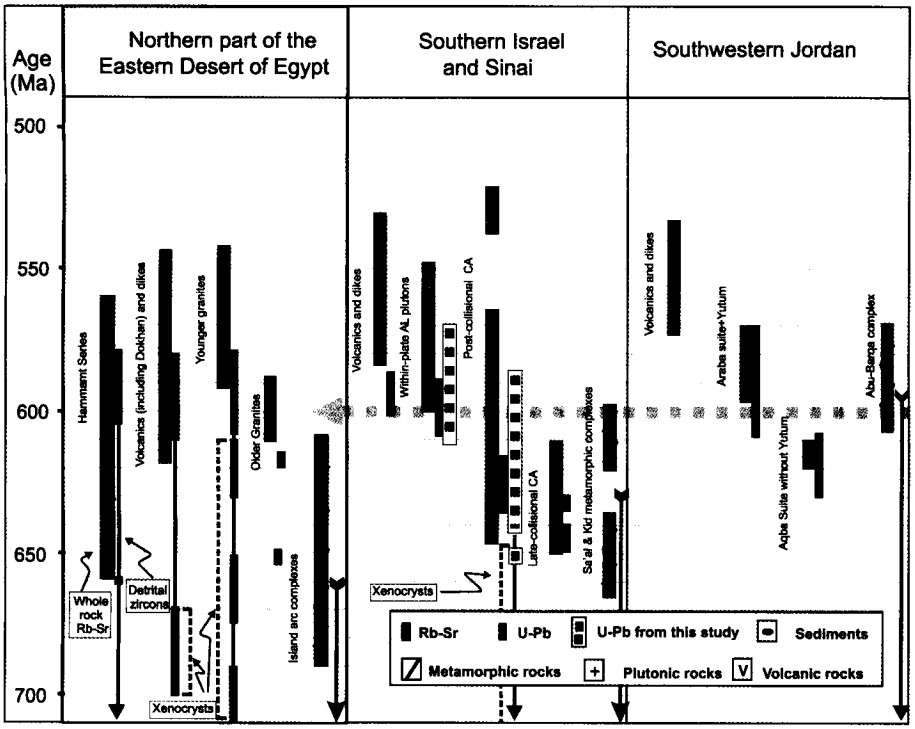

Fig. 8. Compilation of reported ages (U–Pb and Rb–Sr) of rocks from the late evolutionary stages of the northernmost Arabian–Nubian Shield (after Halpern & Tristan 1981; Bielski 1982; Jarrar *et al.* 1983, 2003, and references therein, 2004; Stern & Hedge 1985; Stern & Manton 1987; Willis *et al.* 1988; Kröner *et al.* 1990; Moghazi *et al.* 1998; Moghazi 1999; Wilde & Youssef 2000, 2001; Eyal *et al.* 2004; Kolodner *et al.* 2006; Moussa *et al.* 2008; this study). The names of rock suites are shown to the left of corresponding Rb–Sr and U–Pb age bars. Age bars include a compilation of all the reported ages for that rock suite that have errors less than 30 Ma, with their assigned 2σ errors. Ages of xenocrystic zircons are shown for magmatic rocks. Black arrows indicate that U–Pb ages for the rock suite are older than 710 Ma. The horizontal grey dashed line represents the inferred Saramuj–Hamat Abadu unconformity of Garfunkel (1999) and Jarrar *et al.* (2003), which is not dated but is constrained by field relationships with rocks of known age.

results of Bielski (1982), Moghazi *et al.* (1998), Eyal *et al.* (2004) and Katzir *et al.* (2007*a*)) shows that in most cases the Rb–Sr ages are only slightly (several million years) younger than the U–Pb ages, probably because of the lower closure temperature of the Rb–Sr system. However, some reported Rb–Sr ages (e.g. the *c.* 600 Ma Elat-granite of Halpern & Tristan (1981)), are younger than the determined U–Pb age of the same rocks by more than 20 Ma (Elat-Shlomo (number 1), Elat-Rehavam (number 2), *c.* 630 Ma; Table 1). A more severe problem arises when comparing some reported Rb–Sr ages of metamorphic rocks with the new U–Pb ages in this study. The age of the Kid metamorphic complex was constrained by Halpern & Tristan (1981) and Bielski (1982) to *c.* 600–620 Ma (Rb–Sr, Fig. 8). However, the undeformed Shahira pluton of 632 ± 2 Ma (Table 1) intrudes this complex, implying a minimum age of *c.* 632 Ma for the Kid metamorphic complex. Moreover, U–Pb ages for metavolcanics (770 ± 150 Ma) and granitic pebbles within metasediments (848 ± 61 Ma; 735 ± 25 Ma) of the Kid complex were reported by Blasband *et al.* (1997). Caution should thus be taken when interpreting the reported Rb–Sr age record for the rocks of the northern Arabian–Nubian Shield (see also discussion by Wilde & Youssef 2000). Although we did not date some plutons (or volcanic rocks) for which Rb–Sr ages younger than *c.* 580 Ma were reported in Sinai and southern Israel (Halpern & Tristan 1981; Bielski 1982; Mushkin *et al.* 2003), we found no evidence for magmatic activity younger than *c.* 580 Ma within the 24 dated plutons. Furthermore, all reported U–Pb ages for Neoproterozoic plutonic and volcanic rocks within the northernmost Arabian–Nubian Shield (Fig. 8) as well as U–Pb dating of dykes from southern Israel (Y. Be'eri-Shlevin, unpubl. data) are older than *c.* 580 Ma. With the exception of minor mafic dyke magmatism that may be younger than *c.* 580 Ma (as implied by field relations of these dykes with dated rocks of *c.* 590 Ma), we suggest that the majority of magmatic activity, both plutonic and volcanic, ceased by *c.* 580 Ma, in apparent contrast to some reported younger Rb–Sr ages (Fig. 8).

Timing of magmatism and the transition from CA2 to AL suites

The 24 dated plutons span a wide compositional range of gabbros to granites and are grouped into two major suites according to their chemical affinities (Figs 2–5). CA2 magmatism is constrained to *c.* 635–590 Ma and AL magmatism to *c.* 608–580 Ma (Fig. 7a, Table 1). The variation of magma volume and composition with age in southern Israel and Sinai in Late Neoproterozoic times is shown in Figure 7b. The volume of magma added to the batholith during a certain time interval is calculated by assuming that (1) the surface exposure of a pluton of that age is representative of a slice through a *c.* 30 km thick crust, (2) our sampling set is representative of the different compositional rock types within the CA2 and AL suites in the study area, and (3) undated plutons in Sinai and southern Israel have approximately the same age as dated plutons of similar composition and character.

Similar to other documented post-collisional settings worldwide (Liégeois 1998; Bonin 2004; Jahn 2004), the post-collisional period in the northern Arabian–Nubian Shield (<635 Ma) is characterized by voluminous, mainly high-K calc-alkaline magmatism (Figs 2a and 7b). Diverse mantle and crustal sources have been suggested for post-collisional mafic and felsic magmas in several Phanerozoic orogens, and the source variability has been attributed to the complex pre-collision history (Sylvester 1998; Bonin 2004). However, because subduction and terrane accretion in the northernmost Arabian–Nubian Shield involved almost entirely juvenile components, the radiogenic isotope ratios of the post-collisional rocks are nearly uniform (e.g. $\varepsilon Nd(t) = +2.5$ to $+6.5$; Stein & Goldstein 1996; Stern 2002; Stein 2003; Moussa *et al.* 2008) and can be ambiguously interpreted to derive from either mantle or juvenile crust sources. Thus, unveiling the magma and heat sources for the formation of the vast post-collisional CA2 batholith in the northern Arabian–Nubian Shield awaits further geochemical and isotope (e.g. O, Hf) studies. Nevertheless, regardless of its specific origin, a

Reproduced with permission of the copyright owner. Further reproduction prohibited without permission.

significant feature of the CA2 suite in the northern Arabian–Nubian Shield is the general transition from mafic and intermediate to felsic compositions (Fig. 7a and b). Plutons of gabbro to quartz-diorite composition dominate the early CA2 magmatism at *c.* 632–620 Ma. It should be borne in mind, however, that gabbros are negligible in volume, and that quartz-diorites are generally part of zoned plutons with some granodioritic components. Minor early felsic intrusions (*c.* 635–630 Ma) characterize the small area of southern Israel (Fig. 6a), but felsic magmatism of the CA2 suite (granodiorites and monzogranites) became volumetrically important only at *c.* 610–590 Ma, with a peak around 610–600 Ma (Fig. 6a and b). The abundance of microgranular mafic enclaves in several late CA2 felsic intrusions may indicate that influx of mafic magma into the crust continued, although in reduced quantities, during the dominantly felsic stage of the CA2 suite. However, at this stage, mafic magmas do not form distinct plutons but intermingle with the more dominant felsic magmas. An equally long (350–310 Ma) temporal trend from mafic to felsic calc-alkaline magmatism was also recognized in the post-Variscan batholiths of central Spain (Bea *et al.* 1999). Such trends may be explained by a general decrease in the temperature of the lithosphere following a major orogenic event that involved significant heating. At the earliest stage temperatures were high enough to induce mantle melting; however, as cooling of the lithosphere continued, melting migrated to progressively shallower levels and may have involved partial melting of mafic lower crust as suggested by Jarrar *et al.* (2003) and Stein (2003) for the northern Arabian–Nubian Shield. The intrusion of some evolved CA2 granites at the late post-collisional stage might be interpreted in terms of ponding and differentiation in large mafic magma chambers. However, the importance of this process in generating the voluminous CA2 felsic magmatic pulse (610–590 Ma) is limited, as it requires a huge reservoir of residual mafic material, as yet unidentified in the northern Arabian–Nubian Shield. The scarcity of peraluminous granites and the lack of inheritance in most plutons dated in this study of the northern Arabian–Nubian Shield also rule out a significant contribution from upper crustal (sedimentary) sources.

Although the general trend of the CA2 suite is from mafic to felsic magmatism, some minor felsic intrusions in southern Israel are dated as early as *c.* 635–630 Ma (Fig. 7a). These early felsic magmas may be explained by limited anatexis at mid-crustal levels induced by heat transferred from early mafic magmas. This interpretation is supported by inheritance patterns of some of these granites (see also discussion below).

The *c.* 608–580 Ma AL suite is of decreased volume compared with the CA2 suite (Fig. 7b), but it is widespread throughout the study area (Fig. 1). Alkaline and peralkaline granites do not form distinct age-groups and intrude contemporaneously throughout *c.* 608–580 Ma. Thus alkaline and peralkaline granites may represent variable degrees of differentiation of similar parental magmas, as has been demonstrated in several within-plate magmatic provinces (Zanvilevich *et al.* 1995; Whalen *et al.* 1996; Litvinovsky *et al.* 2002; Jahn 2004). It is also noteworthy that two large AL granites (Sahara (number 15; 240 km^2) and Sharm (number 20; 200 km^2), Fig. 1) intruded at *c.* 10–20 Ma age difference (Fig. 6), but are only *c.* 6 km apart, pointing to a prolonged activity of AL magmatism even within a very localized area. The abundance of bimodal alkaline dykes and volcanic rocks and the dominance of alkaline clasts in molasse-filled intramontane basins demonstrate the association of alkaline magmas with extensional tectonics (Stern *et al.* 1984; Garfunkel 1999; Jarrar *et al.* 2003). Based on geochemical and isotope characteristics, alkaline magmatism was shown to be mantle derived (Beyth *et al.* 1994; Moghazi 1999; Kessel *et al.* 1998; Mushkin *et al.* 2003; Katzir *et al.* 2007*b*). It was thus argued that crustal thinning associated with extension allowed deep, mantle-derived alkaline melts to ascend close to the surface. The new U–Pb ages indicate the intrusion of some peralkaline and alkaline granites prior to the 'Saramuj' or 'Hamat Abadu' unconformity of *c.* 600 Ma described in various localities in the northern Arabian–Nubian Shield (Bentor 1985; Garfunkel 1999; Jarrar *et al.* 2003, and references therein). This is also manifested by the fact that in southern Israel AL plutons and most dykes are unconformably covered by the Elat volcano-conglomerate series, which are cut again by other AL dykes.

The features described above, together with the fact that a *c.* 20 Ma interval of AL magmatism is shown here to overlap with voluminous CA2 felsic magmatism, some 25–40 Ma after this phase began, indicate that a significant portion of CA2 magmatism was also synextensional. Thus felsic AL and CA2 magmas were produced at the same tectonic setting probably from different levels of the lithosphere. Coexistence of CA2 and AL magma chambers may have also involved mixing, giving rise to plutons of transitional character (Malaha pluton (number 13)?).

The intrusion of large, mostly syenogranite plutons associated with ring dyke complexes (Katharina (number 23, *c.* 250 km^2) and Iqna (number 24, *c.* 200 km^2); Table 1, Figs 1 and 7a,b) at *c.* 580 Ma may imply that a second pulse of extension-induced magmatism took place some 30 Ma after the beginning of AL magmatism.

Inheritance

The pattern of zircon inheritance within the 24 dated plutons reflects the sources of these magmas and their interaction with the existing felsic crust at the time of intrusion. The lack of zircon xenocrysts indicates that interaction and assimilation of older felsic crust by magmas of both CA2 and AL suite is very minor. The scarcity of inheritance in these magmas also supports the notion that these are mantle or mafic lower-crustal melts and that a mid-crustal anatexis component is very minor. The presence of zircons with age spectra corresponding to the older island arc complexes is limited to the northeastern part of the study area, at northeastern Sinai and southern Israel (Elat-granites (numbers 1 and 2) and Zreir (number 5) pluton, Table 1). This may indicate a more enhanced interaction of magmas with the 820–740 Ma island arc crust in this region compared with the more southern and western regions. The age range of xenocrystic zircon from these plutons (*c.* 780–900 Ma) compares well with reported ages of the pelitic–psammitic Elat schist that is intruded by the Elat-granites (Kröner *et al.* 1990; Kolodner *et al.* 2006); however, the 900 Ma age is slightly older. Interestingly, xenocrysts of 710–610 Ma detected in younger granites of *c.* 605–595 Ma in the Eastern Desert of Egypt (Moussa *et al.* 2008) were not detected in this study.

Whereas pre Pan-African (pre *c.* 900–950 Ma) ages of inherited zircons incorporated by magmas were reported for more southern parts of the Arabian–Nubian Shield (Sultan *et al.* 1990; Hargrove *et al.* 2006), the age range of the rare xenocrysts in this study, *c.* 607–900 Ma, does not exceed the known age of the Arabian–Nubian Shield crust. The absence of older continental components within this part of the juvenile Arabian–Nubian Shield is thus reaffirmed.

Reproduced with permission of the copyright owner. Further reproduction prohibited without permission.

Tectonic implications

The timing of cessation of subduction, final amalgamation of Gondwana, and the development of extensional features such as core complexes and molasse-filled basins in the northern Arabian–Nubian Shield has been a subject of recent debate (Greiling *et al.* 1994; Stern 1994; Garfunkel 1999; Blasband *et al.* 2000; Katz *et al.* 2004; Doebrich *et al.* 2007).

Doebrich *et al.* (2007) suggested that arc formation and accretionary processes in the Arabian shield were still continuing into the latest Neoproterozoic (620–600 Ma). However, in the northernmost Arabian–Nubian Shield no evidence for arc formation at this stage is evident. The lack of accretionary prisms and other features associated with subduction, such as paired metamorphic belts and linear alignment of calc-alkaline intrusions and volcanic rocks, points to a post-collisional setting at this stage. This conclusion is strengthened by the post-collisional geochemical affinity of most CA2 (and AL) intrusions (Fig. 3a). Although most CA1 and CA2 rocks have subduction-related chemical features (such as negative Nb anomalies), several workers have shown that such features can be explained by the melting of previously formed lithospheric components generated in a subduction-related environment (Friz-Töpfer 1991; Stein *et al.* 1997). Interestingly, Jarrar *et al.* (2003) favoured a subduction-related environment for the oldest calc-alkaline intrusions of the Aqaba suite (equivalent to the CA1 suite), but suggested melting of an amphibolitic lower crust for the later felsic intrusions of the Aqaba suite (equivalent of the CA2 suite). It is important to note that Katz *et al.* (2004) have shown that schistose (greenschist-facies) mafic dykes of southern Israel (*c.* 630 Ma), are high-magnesium andesites similar to low-Ca boninites, which form today only in active subduction zones. Nevertheless, the extent of such magmatism is restricted, and its timing is exactly at the transition between the CA1 and CA2 suites. Moreover, the localized deformation at *c.* 630 Ma of these dykes (Katz *et al.* 2004) is well within the time frame depicted here for the decay of penetrative deformation in the region. Thus the high-magnesium dykes may indicate final, small-scale subduction processes at the transition to post-collisional setting in this region. Likewise, Garfunkel (1999) described the CA2 granitoids of southern Israel (ranging in age from *c.* 635 to 630 Ma) as slightly deformed, and hence probably recording the final decay of deformation until *c.* 625 Ma.

The timing of tectonic and metamorphic events previously related to very late stages in the evolution of the northern Arabian–Nubian Shield should be reconsidered in view of the new geochronology presented here, as follows.

(1) Blasband *et al.* (2000) suggested that extension in the Kid core complex was active until *c.* 580 Ma based on reported Rb–Sr ages of intruding A-type granites of this age (Moghazi *et al.* 1998). In this study we show that a wide range of undeformed mafic to felsic plutons of the CA2 suite that intruded this complex have U–Pb ages of *c.* 630–607 Ma. Thus a minimum age of *c.* 630 Ma is assigned for the Kid core complex.

(2) Cosca *et al.* (1999) suggested that a metamorphic event responsible for most of the deformation recorded in the metamorphic rocks of the northern Arabian–Nubian Shield took place at 620 ± 10 Ma based on their $^{40}Ar/^{39}Ar$ data from southern Israel. However, it is hard to see how the earliest undeformed calc-alkaline plutons dated in this study (636–630 Ma) escaped such widespread metamorphism and penetrative deformation in the northern Arabian–Nubian Shield. The relative scarcity of CA1 (670–625 Ma) deformed plutons and volcanic rocks makes the reconstruction of the final stages of collision within the northernmost Arabian–Nubian Shield difficult. However, in view of the new U–Pb ages for undeformed CA2 and AL rocks, it is clear that penetrative deformation, either compressional (associated with collision) or extensional (associated with core complex doming), had ceased by *c.* 630–625 Ma in this area.

The tectonic evolution of the northernmost Arabian–Nubian Shield as portrayed here (see Fig. 1, inset) is clearly different from that of more southern segments of the Arabian–Nubian Shield, and the inferred correlation between core complexes in these areas (Blasband *et al.* 1997, 2000) is problematic. Whereas the Kid core complex is constrained here to evolve at <630 Ma, core complexes in the southern parts of the Eastern Desert of Egypt were truly active until *c.* 595–575 Ma (Greiling *et al.* 1994, and references therein). The continuation of penetrative deformation in this region until *c.* 580 Ma is supported by the U–Pb ages of deformed plutonic rocks (Nakhil gneisses of Sultan *et al.* 1990). Stern & Hedge (1985) also pointed to the differences in tectonomagmatic evolution of northern, central and southern parts of the Eastern Desert of Egypt. Whereas a syntectonic granodiorite of *c.* 615 Ma was affected by shear in the Meatiq core complex (central Eastern Desert of Egypt), granodiorites of the same age in the northern Eastern Desert of Egypt record no deformation (Stern & Hedge 1985). Another important difference between the northern Arabian–Nubian Shield and more southerly segments is the occurrence of mega-shear zones in the south, such as the Najd fault system, which cannot be traced into the northern Arabian–Nubian Shield. Thus the association of core complexes, shear zones and other extensional features overlapping in time (Greiling *et al.* 1994) in the more southern part of the Arabian–Nubian Shield is not recognized in the north. In contrast, the northern Arabian–Nubian Shield is characterized by major calc-alkaline batholithic magmatism of *c.* 635–590 Ma (postdating an early extensional event?) and a second extensional phase that was associated with the transition to alkaline A-type magmatism at *c.* 600 Ma (Bentor 1985; Beyth *et al.* 1994; Cosca *et al.* 1999; Garfunkel 1999).

Conclusions

(1) The timing of the post-collisional CA2 and within-plate AL magmatism in Sinai and southern Israel is constrained to *c.* 635–590 Ma and *c.* 608–580 Ma, respectively. No trace of younger magmatic events suggested by Rb–Sr dating (560–530 Ma) was found within the 24 dated plutons. The compilation of the reported U–Pb ages in the northern Arabian–Nubian Shield, along with our new U–Pb age spectra, indicates that magmatism younger than *c.* 580 Ma is probably restricted to minor mafic dyke injection.

(2) Within the CA2 suite a change from minor mafic–intermediate to voluminous felsic magmatism took place during a period of *c.* 40–45 Ma, and is interpreted to represent migration of the melting zone from the mantle to lower-crustal levels. This may be interpreted to document a general decrease in the temperature of the lithosphere following a major orogenic event that involved significant heating. Minor felsic crustal anatexis induced by early mafic magmatism may be documented by the early (635–630 Ma) felsic intrusions of southern Israel.

(3) The AL suite comprising mainly alkaline and peralkaline granites, mafic to felsic dykes and associated volcanic rocks is associated by field evidence with extensional tectonics. Significantly, some plutons of this suite intruded prior to the main, Saramuj–Hamat Abadu unconformity of *c.* 600 Ma, thus implying that the extensional tectonic regime may have started prior to *c.* 608 Ma. Alkaline and peralkaline granites do not form distinct

Reproduced with permission of the copyright owner. Further reproduction prohibited without permission.

age-groups; this finding supports their formation via variable degrees of differentiation from similar parental magmas. The intrusion of large, mostly syenogranite plutons associated with ring dyke complexes at *c.* 580 Ma may imply that a second pulse of extension-induced magmatism took place some 30 Ma after the beginning of AL magmatism.

(4) A major discovery of this study is the overlap between a major pulse of felsic CA2 magmatism and the onset of AL magmatism during the range *c.* 608–590 Ma. This suggests that a large proportion of CA2 magmas were also intruded in a synextensional environment. The two suites probably represent different magma-source regions; however, CA2 and AL magma chambers existed coevally at different levels of lithosphere and some interaction between them may have occurred.

(5) The majority of rocks dated in this study show minor to non-existent inheritance, implying minor interaction of the CA and AL magmas with the older island arc crust existing at that time. The age of all zircon xenocrysts analysed in this study ranges from *c.* 607 to 900 Ma. Thus, in contrast to more southerly areas within the Arabian–Nubian Shield, no evidence for continental crust older than known ages of the juvenile Arabian–Nubian Shield is documented in the northernmost part of the Arabian–Nubian Shield.

(6) In most of the northernmost Arabian–Nubian Shield, including the northern Eastern Desert of Egypt, Sinai, southern Israel and southwestern Jordan, penetrative deformation had mainly ceased by *c.* 630 Ma, and its decay until 625 Ma is recorded in some slightly deformed rocks. This is also the time at which subduction ended in this region. We infer that the northernmost Arabian–Nubian Shield, and its more southerly counterparts, experienced a different tectonic evolution during the time span of *c.* 630–580 Ma. Whereas in the south core complexes and mega-shear zones are documented to be active until 580–570 Ma, these cannot be traced in the northernmost Arabian–Nubian Shield. In contrast, this region is characterized by major calc-alkaline batholithic magmatism of *c.* 635–590 Ma shifting to an extensional phase that was associated with the transition to alkaline A-type magmatism at *c.* 600 Ma.

This study was funded by a HIGH-LAT grant of the European Commission's Improving Human Potential Program, a SYNTHESYS grant of the European Commission's FPVI European-funded Integrated Infrastructure Initiative and by Israel Science Foundation grant 142/02. We thank M. Eyal for sharing with us his geochemical database of the Sinai rocks, and A. Gal-Steinitz for the Timna zircon samples. We also wish to thank T. Glickstein and Y. and O. Malmud for their help in sampling, and G. Tirosh for help with sample handling. Z. Brener and U. Krammer of Universitat Karlsruhe are thanked for geochemical analysis of several samples. This paper benefited from numerous stimulating discussions with B. Litvinovsky, A. Zanvilevich and M. Eyal, and from thorough reviews of an earlier version by C. Frost, R. Stern and S. Wilde. Constructive comments by two anonymous referees and editor A. Collins helped to improve this paper.

References

Bea, F., Montero, P. & Molina, J.F. 1999. Mafic precursors, peraluminous granitoids, and late lamprophyres in the Avila batholith: A model for the generation of Variscan batholiths in Iberia. *Journal of Geology*, **107**, 399–419.

Bentor, Y.K. 1985. The crustal evolution of the Arabian–Nubian Massif with special reference to the Sinai Peninsula. *Precambrian Research*, **28**, 1–74.

Bentor, Y.K. & Eyal, M. 1987. *The geology of southern Sinai, its implication for the evolution of the Arabian–Nubian Massif.* Israel Academy of Science Humanities, Jerusalem.

Beyth, M., Stern, R., Altherr, R. & Kröner, A. 1994. The late Precambrian Timna igneous complex, Southern Israel: evidence for comagmatic-type sanukitoid monzodiorite and alkali granite magma. *Lithos*, **31**, 103–124.

Bielski, M. 1982. *Stages in the evolution of the Arabian–Nubian massif in Sinai.* PhD thesis, Hebrew University of Jerusalem.

Blasband, B., Brooijmans, P., Dirks, P., Visser, W. & White, S. 1997. A Pan-African core complex in the Sinai, Egypt. *Geologie en Mijnbouw*, **73**, 247–266.

Blasband, B., White, S., Brooijmans, P., De Boorder, H. & Visser, W. 2000. Late Proterozoic extensional collapse in the Arabian–Nubian Shield. *Journal of the Geological Society, London*, **157**, 615–628.

Bonin, B. 2004. Do coeval mafic and felsic magmas in post-collisional to within-plate regimes necessarily imply two contrasting, mantle and crustal, sources? A review. *Lithos*, **78**, 1–24.

Cosca, M.A., Shimron, A. & Caby, R. 1999. Late Precambrian metamorphism and cooling in the Arabian–Nubian Shield: Petrology and $^{40}Ar/^{39}Ar$ geochronology of metamorphic rocks of the Elat area (southern Israel). *Precambrian Research*, **98**, 107–127.

Corfu, F., Hanchar, J.M., Hoskin, P.W.O. & Kinny, P. 2003. Atlas of zircon textures. *In:* Hanchar, J.M. & Hoskin, P.W.O. (eds) *Zircon*. Mineralogical Society of America, Reviews in Mineralogy and Geochemistry, **53**, 469–500.

Doebrich, J.L., Al-Jehani, A.M., Siddiqui, A.A., Hayes, T.S., Wooden, J.L. & Johnson, P.R. 2007. Geology and metallogeny of the Ar Rayn terrane, eastern Arabian shield: Evolution of a Neoproterozoic continental-margin arc during assembly of Gondwana within the East African Orogen. *Precambrian Research*, **158**, 17–50.

Eyal, M., Bartov, Y., Shimron, A.E. & Bentor, Y.K. 1980. *Sinai geological map 1:500 000 scale.* Geological Survey of Israel, Jerusalem.

Eyal, M., Litvinovsky, B.A., Katzir, Y. & Zanvilevich, A.N. 2004. The Pan-African high-K calk-alkaline peraluminous Elat granite of southern Israel: geology, geochemistry and petrogenesis. *Journal of African Earth Sciences*, **40**, 115–136.

Friz-Töpfer, A. 1991. Geochemical characterization of Pan-African dyke swarms in southern Sinai: from continental margin to intraplate magmatism. *Precambrian Research*, **49**, 281–300.

Frost, B.R., Barnes, C.G., Collins, W.J., Arculus, R.J., Ellis, D.J. & Frost, C.D. 2001. A geochemical classification for granitic rocks. *Journal of Petrology*, **42**, 2033–2048.

Garfunkel, Z. 1999. History and paleogeography during the Pan-African orogen to stable platform transition: Reappraisal of the evidence from Elat area and the northern Arabian–Nubian Shield. *Israel Journal of Earth Sciences*, **48**, 135–157.

Greiling, R.O., Abdeen, M.M., Dardir, A.A., *et al.* 1994. A structural synthesis of the Proterozoic Arabian–Nubian Shield in Egypt. *Geologische Rundschau*, **83**, 484–501.

Halpern, M. & Tristan, N. 1981. Geochronology of the Arabian–Nubian Shield in southern Israel and eastern Sinai. *Journal of Geology*, **89**, 639–648.

Hargrove, U.S., Stern, R.J., Kimura, J.-I., Manton, W.I. & Johnson, P.R. 2006. How juvenile is the Arabian–Nubian Shield? Evidence from Nd isotopes and pre-Neoproterozoic inherited zircon in the Bi'r Umq suture zone, Saudi Arabia. *Earth and Planetary Science Letters*, **252**, 308–326.

Hoskin, P.W.O. & Schaltegger, U. 2003. The composition of zircon and igneous and metamorphic petrogenesis. *In:* Hanchar, J.M. & Hoskin, P.W.O. (eds) *Zircon*. Mineralogical Society of America, Reviews in Mineralogy and Geochemistry, **53**, 27–62.

Jahn, B.-M. 2004. The Central Asian Orogenic Belt and growth of the continental crust in the Phanerozoic. *In:* Malpas, J., Fletcher, C.J.N., Ali, J.R. & Aitchison, J.C. (eds) *Aspects of the Tectonic Evolution of China*. Geological Society, London, Special Publications, **226**, 73–100.

Jarrar, G., Baumann, A. & Wachendorf, H. 1983. Age determinations in the Precambrian basement of the Wadi Araba area, southwest Jordan. *Earth and Planetary Science Letters*, **63**, 292–304.

Jarrar, G., Stern, R.J., Saffarini, G. & Al-Zubi, H. 2003. Late- and post-orogenic Neoproterozoic intrusions of Jordan: implications for crustal growth in the northernmost segment of the East African Orogen. *Precambrian Research*, **123**, 295–319.

Jarrar, G., Saffarini, G., Wachendorf, H. & Baumann, A. 2004. Origin, age and petrogenesis of Neoproterozoic composite dykes from the Arabian–Nubian Shield, SW Jordan. *Geological Journal*, **39**, 157–178.

Katz, O., Avigad, D., Matthews, A. & Heimann, A. 1998. Precambrian metamorphic evolution of the Arabian–Nubian Shield in the Roded area, southern Israel. *Israel Journal of Earth Sciences*, **47**, 93–110.

Katz, O., Beyth, M., Miller, N., Stern, R., Avigad, D., Basu, A. & Anbar, A. 2004. A Late Neoproterozoic (*c.* 630 Ma) high-magnesium andesite suite from southern Israel: implications for the consolidation of Gondwanaland. *Earth and Planetary Science Letters*, **218**, 275–290.

Katzir, Y., Litvinovsky, B.A., Jahn, B.M., Eyal, M., Zanvilevich, A.N. & Vapnik, Ye. 2006. Four successive episodes of Late Pan-African dykes in the central Elat area, southern Israel. *Israel Journal of Earth Sciences*, **55**, 69–93.

Reproduced with permission of the copyright owner. Further reproduction prohibited without permission.

KATZIR, Y., EYAL, M., LITVINOVSKY, B.A., *ET AL.* 2007*a*. Petrogenesis of A-type granites and origin of vertical zoning in the Katharina pluton, area of Gebel Mussa (Mt. Moses), Sinai, Egypt. *Lithos*, **95**, 208–228.

KATZIR, Y., LITVINOVSKY, B.A., JAHN, B.M., *ET AL.* 2007*b*. Interrelations between coeval mafic and A-type silicic magmas from composite dykes in a bimodal suite of southern Israel, northernmost Arabian–Nubian Shield: Geochemical and isotope constraints. *Lithos*, **97**, 336–364.

KESSEL, R., STEIN, M. & NAVON, O. 1998. Petrogenesis of late Neoproterozoic dykes in the northern Arabian–Nubian Shield. Implications for the origin of A-type granites. *Precambrian Research*, **92**,195–213.

KOLODNER, K., AVIGAD, D., MCWILLIAMS, M., WOODEN, J.L., WEISSBROD, T. & FEINSTEIN, S. 2006. Provenance of north Gondwana Cambrian–Ordovician sandstone: U–Pb SHRIMP dating of detrital zircons from Israel and Jordan. *Geological Magazine*, **143**, 367–391.

KRÖNER, A., EYAL, M. & EYAL, Y. 1990. Early Pan-African evolution of the basement around Elat, Israel, and Sinai Peninsula revealed by single-zircon evaporation dating, and implications for crustal accretion rates, *Geology*, **18**, 545–548.

LEE, J. & WHITEHOUSE, M.J. 2007. Onset of mid-crustal extensional flow in southern Tibet: Evidence from U/Pb zircon ages. *Geology*, **35**, 45–48.

LIÉGEOIS, J.P. 1998. Prefaces—some words on post-collisional magmatism. *Lithos*, **45**, 15–17.

LITVINOVSKY, B. A., JAHN, B.-M., ZANVILEVICH, A.N., SAUNDERS, A. & POULAIN, S. 2002. Petrogenesis of syenite–granite suites from the Bryansky Complex (Transbaikalia, Russia): implications for the origin of A-type granitoids magmas. *Chemical Geology*, **189**, 105–133.

LUDWIG, K.R. 2001. Isoplot/Ex rev. 2.49. A geochronological toolkit for Microsft Excel. *Berkeley Geochronology Center, Special Publications*, **1a**.

MCLAREN, A.C., FITZGERALD, J.D. & WILLIAMS, I.S. 1994. The microstructure of zircon and its influence on the age determination from Pb/U isotopic ratios measured by ion microprobe. *Geochimica et Cosmochimica Acta*, **58**, 993–1005.

MEERT, J.G. 2003. A synopsis of events related to the assembly of eastern Gondwana. *Tectonophysics*, **362**, 1–40.

MOGHAZI, A.M. 1999. Magma source and evolution of Late Neoproterozoic granitoids in the Gabal El-Urf area, eastern Desert, Egypt: geochemical and Sr–Nd isotopic constraints. *Geological Magazine*, **136**, 285–300.

MOGHAZI, A.M., ANDERSON, T., OWEISS, G.A. & EL BOUSELLY, A.M. 1998, Geochemical and Sr–Nd–Pb isotopic data bearing on the origin of Pan-African granitoids in the Kid area, southeast Sinai, Egypt. *Journal of the Geological Society, London*, **155**, 697–710.

MOUSSA, M.M.E., STERN, J.R., MANTON, W.I. & ALI, K.A. 2008. SHRIMP zircon dating and Sm/Nd isotopic investigations of Neoproterozoic granitoids, Eastern Desert, Egypt. *Precambrian Research*, **160**, 341–356.

MUSHKIN, A., NAVON, O., HALITZ, L., HEIMANN, A., HARTMANN, G. & STEIN, M. 2003. The petrogenesis of A-type magmas from the Amram Massif, southern Israel. *Journal of Petrology*, **44**, 815–832.

PEARCE, J.A., HARRIS, N.B.W. & TINDLE, A.G. 1984. Trace element discrimination diagrams for the tectonic interpretation of granitic rocks. *Journal of Petrology*, **25**, 956–983.

PEARCE, J.A. 1996. Sources and settings of granitic rocks. *Episodes*, **19**, 120–125.

RICKWOOD, P.C. 1989. Boundary lines within petrologic diagrams which use oxides of major and minor elements. *Lithos*, **22**, 247–263.

STACEY, J.S. & KRAMERS, J.D. 1975. Approximation of terrestrial lead isotope evolution by a 2-stage model. *Earth and Planetary Science Letters*, **26**, 207–221.

STEIGER, R.H. & JÄGER, E. 1977. Subcommision on geochronology: convention of the use of decay constants in geo- and cosmo-chronology. *Earth and Planetary Science Letters*, **36**, 359–362.

STEIN, M. 2003. Tracing the plume material in the Arabian–Nubian Shield. *Precambrian Research*, **123**, 223–234.

STEIN, M. & GOLDSTEIN, S. 1996. From plume head to continental lithosphere in the Arabian–Nubian Shield. *Nature*, **382**, 773–778.

STEIN, M., NAVON, O. & KESSEL, R. 1997. Chromatographic metasomatism of the Arabian–Nubian lithosphere. *Earth and Planetary Science Letters*, **152**, 75–91.

STERN, R.J. 1994. Arc assembly and continental collision in the Neoproterozoic East African Orogen: Implications for the consolidation of Gondwanaland. *Annual Review of Earth and Planetary Sciences*, **22**, 319–351.

STERN, R.J. 2002. Crustal evolution in the East African Orogen: a neodymium isotopic perspective. *Journal of African Earth Sciences*, **34**, 109–117.

STERN, R.J., GOTTFRIED, D. & HEDGE, C.E. 1984. Late Precambrian rifting and crustal evolution in the northeast Desert of Egypt. *Geology*, **12**, 168–172.

STERN, R.J. & HEDGE, C.E. 1985. Geochronologic and isotopic constraints on Late Proterozoic crustal evolution in the Eastern Desert of Egypt. *American Journal of Science*, **285**, 97–127.

STERN, R.J. & MANTON, W.I. 1987. Age of Feiran basement rocks, Sinai: implications for late Precambrian crustal evolution in the northern Arabian–Nubian Shield. *Journal of the Geological Society, London*, **144**, 569–575.

STOESER, D.B. & FROST, C.D. 2006. Nd, Pb, Sr, and O isotopic characterization of Saudi Arabian Shield terranes. *Chemical Geology*, **226**, 163–188.

SULTAN, M., CHAMBERLAIN, K.R., BOWRING, S.A., ARVIDSON, R.E., ABUZIED, H. & EL KALIOUBY, B. 1990. Geochronologic and isotopic evidence for the involvement of pre-Pan-African crust in the Nubian Shield, Egypt. *Geology*, **18**, 761–764.

SUN, S.-S. & MCDONOUGH, W.F. 1989. Chemical and isotopic systematics of the oceanic basalts: implications for mantle composition and processes. *In:* SAUNDERS, A.D. & NORRY, M.J. (eds) *Magmatism in the Ocean Basins*. Geological Society, London, Special Publications, **42**, 313–345.

SYLVESTER, P.J. 1989. Post-collisional alkaline granites. *Journal of Geology*, **97**, 261–280.

SYLVESTER, P.J. 1998. Post-collisional strongly peraluminous granites. *Lithos*, **45**, 29–44.

WHALEN, J.B., CURRIE, K.L. & CHAPPELL, B.W. 1987. A-type granites: geochemical characteristics, discrimination and petrogenesis. *Contributions to Mineralogy and Petrology*, **95**, 407–419.

WHALEN, J.B., JENNER, J.A., LONGSTAFFE, F.J., ROBERT, F. & GARIEPY, C. 1996. Geochemical and isotopic (O, Nd, Pb, and Sr) constraints on A-type granite petrogenesis based on the Topsails igneous suite, Newfoundland Appalachians. *Journal of Petrology*, **37**, 1463–1489.

WHITEHOUSE, M.J., KAMBER, B. & MOORBATH, S. 1999. Age significance of U–Th–Pb zircon data from early Archean rocks of west Greenland—a reassessment based on combined ion-microprobe and imaging studies. *Chemical Geology*, **160**, 201–224.

WIEDENBECK, M., ALLÉ, P., CORFU, F., *ET AL.* 1995. Three natural zircon standards for U–Th–Pb, Lu–Hf, trace element and REE analysis. *Geostandards Newsletter*, **19**, 1–23.

WILDE, S.A. & YOUSSEF, K. 2000. Significance of SHRIMP U–Pb dating of the Imperial Porphyry and associated Dokhan Volcanics, Gebel Dokhan, north Eastern Desert, Egypt. *Journal of African Earth Sciences*, **31**, 403–413.

WILDE, S.A. & YOUSSEF, K. 2001. SHRIMP U–Pb dating of detrital zircons from the Hammamat Group of Gebel UmmTawat, North-Eastern Desert, Egypt. *Gondwana Research*, **4**, 202–206.

WILLIS, K.M., STERN, R.J. & CLAUER, N. 1988. Age and geochemistry of Late Precambrian sediments of the Hammamat Series from North Eastern Desert of Egypt. *Precambrian Research*, **42**, 173–187.

ZANVILEVICH, A.N., LITVINOVSKY, B.A., WICKHAM, S.M. & BEA, F. 1995. Genesis of alkaline and peralkaline syenite–granite series: the Kharitonovo pluton (Transbaikalia, Russia). *Journal of Geology*, **103**, 127–145.

Received 4 December 2007; revised typescript accepted 21 August 2008.
Scientific editing by Alan Collins.

Reproduced with permission of the copyright owner. Further reproduction prohibited without permission.